AGU PUBLICATIONS

JGR

Journal of Geophysical Research: Atmospheres

RESEARCH ARTICLE
10.1002/2016JD025207

Key Points:
- Noticeable improvements to the ice cloud optical properties are made for the Community Radiative Transfer Model
- Satellite observations and CRTM simulations show better agreements with the updated ice cloud optical properties
- Consistent ice cloud optical properties with polarization covering visible, infrared, and microwave spectrum are provided

Correspondence to:
B. Yi,
bingqi.yi@outlook.com

Citation:
Yi, B., P. Yang, Q. Liu, P. van Delst, S.-A. Boukabara, and F. Weng (2016), Improvements on the ice cloud modeling capabilities of the Community Radiative Transfer Model, *J. Geophys. Res. Atmos.*, *121*, 13,577–13,590, doi:10.1002/2016JD025207.

Received 8 APR 2016
Accepted 10 OCT 2016
Accepted article online 12 OCT 2016
Published online 18 NOV 2016

Improvements on the ice cloud modeling capabilities of the Community Radiative Transfer Model

Bingqi Yi[1], Ping Yang[1], Quanhua Liu[2,3], Paul van Delst[3], Sid-Ahmed Boukabara[3], and Fuzhong Weng[4]

[1]Department of Atmospheric Sciences, Texas A&M University, College Station, Texas, USA, [2]ESSIC, University of Maryland, College Park, Maryland, USA, [3]Joint Center for Satellite Data Assimilation, College Park, Maryland, USA, [4]NOAA/NESDIS/STAR, College Park, Maryland, USA

Abstract Noticeable improvements on the ice cloud modeling capabilities of the Community Radiative Transfer Model (CRTM) are reported, which are based on the most recent advances in understanding ice cloud microphysical (particularly, ice particle habit/shape characteristics) and optical properties. The new CRTM ice cloud model is derived from the Moderate Resolution Imaging Spectroradiometer (MODIS) collection 6 ice cloud habit model, which represents ice particles as severely roughened hexagonal ice column aggregates with a gamma size distribution. The single-scattering properties of the new ice particle model are derived from a state-of-the-art ice optical property library and are constructed as look-up tables for rapid CRTM computations. Various sensitivity studies concerning instrument-specific applications and simulations are performed to validate CRTM against satellite observations. In particular, radiances in a spectral region covering the infrared wavelengths are simulated. Comparisons of brightness temperatures between CRTM simulations and observations (from MODIS, the Atmospheric Infrared Sounder, and the Advanced Microwave Sounding Unit) show that the new ice cloud optical property look-up table substantially enhances the performance of the CRTM under ice cloud conditions.

1. Introduction

Ice clouds covering vast areas over the globe play an important role in the atmospheric radiative transfer processes and climate system [*Liou*, 1986; *Lynch et al*., 2002; *Yang et al*., 2015] due to scattering and absorption of shortwave and longwave radiation by ice particles. For accurate remote sensing retrievals and radiative impact assessment, radiative transfer models must accurately represent ice clouds and their radiative effects, a task that is quite challenging due to the complex nature of ice cloud properties. The nonspherical characteristic habits [*Heymsfield et al*., 2013; *Schmitt and Heymsfield*, 2007; *Ulanowski et al*., 2006], various degrees of surface roughness [*Ulanowski et al*., 2006, 2012], and wide ranges of sizes of ice particles make it difficult to compute the optical properties of ice crystals. In particular, it is critical to define a specific ice cloud particle habit model for use in the radiative transfer model.

Realistic atmospheric ice crystals are so complicated in terms of their morphologies, and it is inevitable to define the particle geometries with simplifications in theoretical studies. In this line, various kinds of ice cloud particle models from simple to quite complicated particle habits have been reported, for example, to name a few, by *Macke et al*. [1996], *Baran et al*. [2014], *Baum et al*. [2005, 2011], *Yang et al*. [2003], *Zhang et al*. [2004], and *Um and McFarquhar* [2007, 2009]. The most widely used ice particle model is a smooth-surface single hexagonal column [*Takano and Liou*, 1989]. In particular, such an ice model (and some further improvements, i.e., consideration of surface roughness) has been used in a wide range of studies in radiative transfer models [*Fu and Liou*, 1993; *Fu*, 1996] and general circulation models [*Ebert and Curry*, 1992; *Mitchell et al*., 1996; *van Diedenhoven et al*., 2014]. More complicated ice models such as ice habit mixture and ice aggregate models [*McFarquhar et al*., 2002; *Nasiri et al*., 2002] that account for ice particle surface roughness features are implemented in ice cloud remote sensing applications, for instance, the general habit mixture model [*Baum et al*., 2011] and the two-habit model [*Liu et al*., 2014]. *Yi et al*. [2013] confirm that these ice habit mixture models give improved performance in ice cloud radiative forcing simulations with broadband radiative transfer models. Although theoretically defined aggregate morphologies may not resemble observed ice crystals, an aggregate model could be an optimal representation of an ensemble of ice particles in terms of their optical properties for practical applications. An appropriate ice aggregate model does not necessarily physically resemble observed ice crystal shapes. In particular, Moderate Resolution Imaging Spectroradiometer (MODIS) collection 5 (MC5) assumes an ice habit mixture model for ice cloud property retrievals [*Baum*

et al., 2005]. The current version of the Community Radiative Transfer Model (CRTM) also uses MC5 as the default ice model for ice cloud condition simulations [*Ding et al*., 2011]. However, MC5 produces inconsistent retrievals in visible and infrared channels. As the MODIS collection 6 (MC6) operational retrievals introduce a new severely roughened hexagonal column aggregate ice model [*Platnick et al*., 2015] that resembles natural ice cloud particles to some extent, in this study we implement the MC6 ice cloud model and perform sensitivity studies toward validating the MC6 model within the CRTM framework.

In the microwave region, the size of ice cloud particle is relatively small compared with the wavelength. Rayleigh scattering approximation could be used below some selected particle size and frequency thresholds [*Schneider and Stephens*, 1995]. Various computational methods, including the finite difference time domain method [e.g., *Yee*, 1966; *Yang and Liou*, 1996b], the discrete dipole approximation [e.g., *Yurkin et al*., 2007], and the T-matrix method [e.g., *Mishchenko and Travis*, 1998], have been employed to calculate the microwave single-scattering properties of nonspherical ice particles. As with visible and infrared wavelengths, different ice particle models are used in the microwave region [*Evans and Stephens*, 1995; *Evans et al*., 1998; *Hong*, 2007a, 2007b; *Liu*, 2008; *Hong et al*., 2009]. In the present CRTM, the microwave ice scattering properties are not based on MC5 but are derived from the Lorenz-Mie theory by assuming spherical ice particles. However, to be consistent with the visible and infrared region, in this study we also extend the implementation of the MC6 ice particle model to the microwave region.

Although the present CRTM does not consider polarization, the doubling-adding radiative transfer solver in CRTM [*Liu and Weng*, 2006] is able to include polarization by expanding to vector radiative transfer. While polarization is important even for radiance simulations involving ice clouds [*Yi et al*., 2014a], this study only discusses unpolarized results. In addition, a set of consistent ice cloud optical properties including complete polarization properties are provided for future developments and improvements of CRTM.

This paper is organized as follows: section 2 describes the new MC6-based ice cloud model, calculation of the relevant optical properties, and the updated CRTM. Section 3 compares the simulations based on the CRTM against observations by multiple satellite sensors. The conclusions of this study are given in section 4.

2. Data and Methodology

2.1. Model and Data Used

The CRTM is developed and maintained by the U.S. Joint Center for Satellite Data Assimilation to support simulation of radiances (and Jacobians) at the top of the atmosphere for various satellite sensors focusing on different spectral channels in the visible to microwave region [*Han et al*., 2006]. The CRTM considers six types of clouds: water cloud, ice cloud, rain cloud, snow cloud, graupel cloud, and hail cloud. This study focuses on ice cloud optical properties using CRTM version 2.1.3 which, as stated above, adopts MC5 as a default ice model.

Satellite ice cloud retrieval products from the operational Aqua MODIS collections 5.1 and 6 data set are employed to support the validation of the CRTM-simulated brightness temperatures against observations. Aqua MODIS level 2 ice cloud optical property retrieval products ("MYD06_L2") include ice water path, cloud particle effective radius [*Platnick et al*., 2003], and cloud top pressure [*Menzel et al*., 2008]. The cloud phase product ("Cloud_Phase_Optical_Properties") is used to discriminate clear-sky, ice cloud, and water cloud conditions [*King et al*., 2010]. Also needed are the source-viewing geometries (solar zenith angle, satellite viewing zenith angle, etc.) and the surface temperature. Modern-era Retrospective Analysis for Research and Applications reanalysis atmospheric profiles [*Rienecker et al*., 2011] are collocated temporally and spatially to each ice cloud pixel to provide basic meteorological parameters such as pressure, temperature, water vapor, and trace gases.

Simultaneous measurements of brightness temperatures from various channels of MODIS and Advanced Microwave Sounding Unit-A (AMSU-A) instruments on board the Aqua satellite are collocated with the MODIS ice cloudy pixels. Hyperspectral brightness temperature observations from the Atmospheric Infrared Sounder (AIRS) are also collocated. These observations are used to validate implementation of the new MC6 ice cloud property look-up table (LUT) in the visible, infrared, and microwave regions.

2.2. Ice Particle Model

The current CRTM default (MC5) [*Ding et al*., 2011] ice habit model is composed of six ice habits including droxtals, bullet rosettes, hexagonal plates, hollow/solid columns, and aggregates, with the ice habit fractions changing with ice particle size. In the present study, we update the CRTM ice cloud model to use the MC6 counterpart, which represents ice particles in terms of severely roughened hexagonal ice column aggregates following the analytical gamma size distribution. The surface roughness of ice particle is achieved by randomly distorting the particle surface slope using a σ parameter, whose physical meaning can be found in *Yang and Liou* [1998]. The σ parameter with a value of 0.5 denotes that the ice particles are severely roughened [*Yang et al*., 2013; *Yi et al*., 2013]. The single-scattering properties corresponding to this severely roughened hexagonal ice column aggregate model are directly derived from a comprehensive library of ice optical properties [*Yang et al*., 2013], containing nine frequently observed ice habits and with explicit consideration of ice particle surface roughness. The database is calculated with the use of the discrete dipole approximation [*Yurkin et al*., 2007] for small particles and the improved geometric optics method [*Yang and Liou*, 1996a; *Bi et al*., 2009; *Bi et al*., 2014] for large particles. The ice optical properties in the microwave spectrum are new additions to the 2013 database computed by using the invariant imbedding T-matrix method [*Bi et al*., 2013; *Bi and Yang*, 2014]. We examine the differences in ice optical properties in the microwave region at two temperatures (160 K and 230 K) because previous studies found considerable dependency of ice optical constants on temperature [e.g., *Iwabuchi and Yang*, 2011].

The gamma size distribution is used for ice cloud in the form

$$n(r) = N_0 r^{\mu} \exp(-\Lambda r) = N_0 r^{(1-3\upsilon_{\text{eff}})/\upsilon_{\text{eff}}} \exp\left(-\frac{r}{r_{\text{eff}}\upsilon_{\text{eff}}}\right), \tag{1}$$

where N_0 is the intercept, μ is the shape parameter, Λ is the slope parameter, r is the maximum dimension of individual particle, r_{eff} is the effective radius, and υ_{eff} is the effective variance (=0.1). The effective radius [*Foot*, 1988] is defined as

$$r_{\text{eff}} = \frac{3}{4}\frac{\int_{r_{\min}}^{r_{\max}} V(r)n(r)dr}{\int_{r_{\min}}^{r_{\max}} A(r)n(r)dr}, \tag{2}$$

where V and A are the volume and projected area and $r_{\min}$ and $r_{\max}$ are the minimum and maximum sizes of the ice particles.

The method to derive the spectral bulk scattering properties of ice cloud is the same as employed in *Yi et al*. [2013, 2014b]. The scattering properties are calculated accurately using the MC6 ice model and, for rapid computation, are organized in the CRTM using the same LUT format as in the current default (MC5) ice model. Specifically, the ice cloud LUT in the visible and infrared region contains 61 wave numbers spanning from 200 to 37037.04 cm^{-1} and 10 effective radii from 2 to 100 μm, while the microwave region covers 31 frequencies from 1.4 to 190.31 GHz and 10 effective radii from 5 to 1500 μm. Because the same ice properties are used for other ice phase hydrometeors with large sizes (e.g., graupel) in the microwave region, the range of effective radii is wider in the microwave region than that in the visible and infrared region.

Figure 1 compares the ice cloud bulk scattering properties between the MC6 and the CRTM default (MC5) ice cloud models. The single-scattering albedo, mass extinction coefficient, and asymmetry factor are plotted as functions of the effective radius and wavelength. The mass extinction coefficient shows a rapid decrease with increasing effective radius when the wavelength is smaller than 10 μm (Figure 1a). However, the MC6 minus MC5 differences in mass extinction coefficient are minimal except at wavelengths around 3 μm, where the difference can be as large as $-0.7\ \text{m}^2\ \text{g}^{-1}$ (Figure 1d). The single-scattering albedo also shows apparent negative differences at wavelengths around 3 μm (Figures 1b and 1e). At wavelengths shorter than 3 μm, the single-scattering albedo approaches 1 with little MC6 minus MC5 difference. For wavelengths larger than 3 μm, positive differences in single-scattering albedo are found at small effective radii. Generally speaking, the largest differences are noted in the asymmetry factor, where MC6 has an almost constant asymmetry factor around 0.75 in the visible spectrum, while MC5 has an increasing asymmetry factor as the effective radius increases (Figures 1c and 1f). At infrared wavelengths, the asymmetry factor approaches 1, especially for large effective radii. Significantly large positive differences ($>$0.2) are found when the wavelength is larger than 10 μm and the effective radius is smaller than 10 μm. Overall, the change in ice particle model induces various

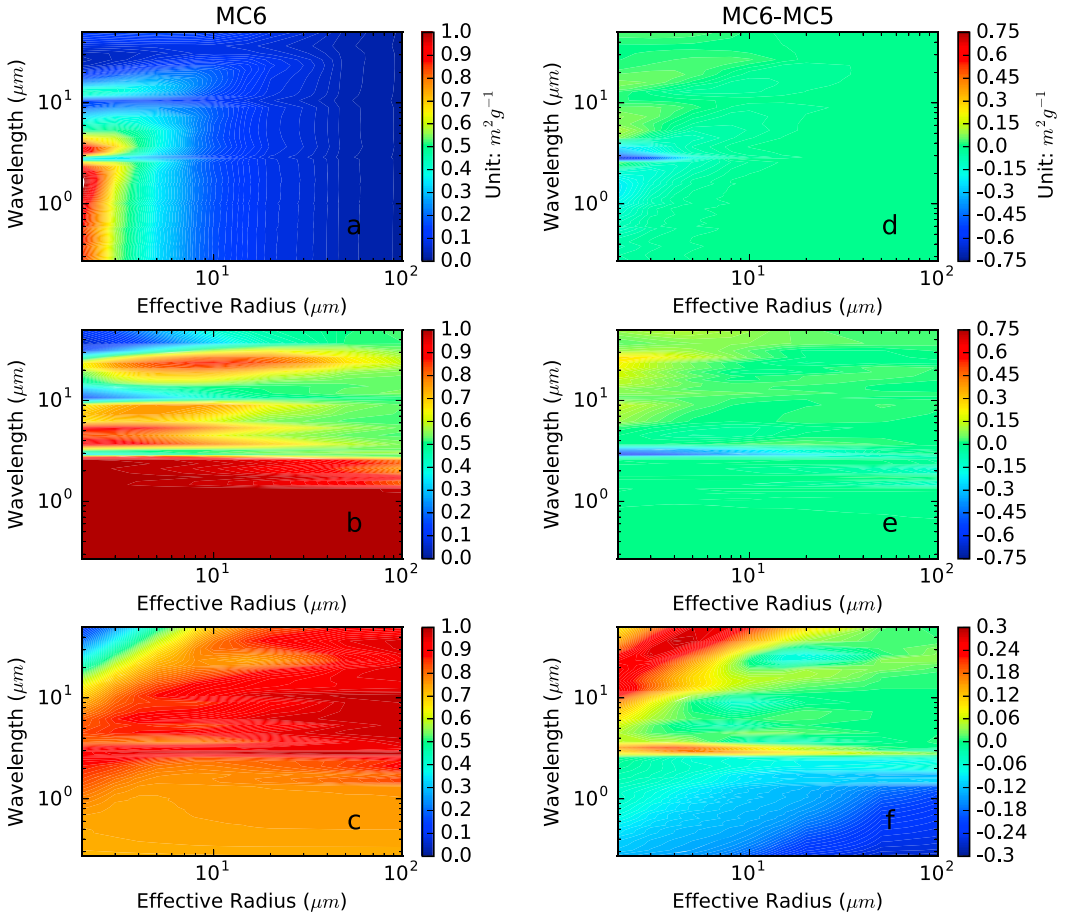

Figure 1. Comparison of bulk optical properties between the new ice cloud model (MC6) and the default (MC5) CRTM ice cloud in the visible and infrared region: (a) mass extinction coefficient, (b) single-scattering albedo, (c) asymmetry factor, and (d–f) the corresponding MC6 minus MC5 differences of Figures 1a–1c.

impacts on the optical properties at the visible and infrared spectra. The differences in ice scattering properties between MC5 and MC6 at certain wavelengths (i.e., 3 μm) may be partially attributed to the different ice refractive indices used in MC5 [*Warren*, 1984] and MC6 [*Warren and Brandt*, 2008] ice models.

Similarly, the mass extinction coefficient, single-scattering albedo, and asymmetry factor as functions of the effective radius and frequency in the microwave region are shown in Figures 2a–2c. Note that the MC6 ice optical property LUTs in microwave region have been constructed under different temperatures. The MC6 mass extinction coefficient (Figure 2a) has a peak region at high frequencies (>150 GHz) and large effective radii (300–700 μm). In the microwave region (in particular, for >50 GHz), the ice single-scattering albedo (Figure 2b) has stronger sensitivity to the particle size. For ice particles with effective radii lower than 20 μm, the single-scattering albedo is lower than 0.3, but by about 40 μm, rapidly increases 0.9. The low-frequency cases (<50 GHz) show a more complicated relation between the single-scattering albedo and the effective radius. The asymmetry factor (Figure 2c), similar to Figure 2a, has a peak value at some large effective radius but with the peak frequency region becoming noticeable between 50 and 100 GHz.

Also illustrated are the corresponding differences between CRTM default and MC6 ice optical properties at 160 K (Figures 2d–2f), as well as the differences between MC6 ice properties at 160 K and those at 230 K (Figures 2g–2i). It is evident that the MC6 and MC5 ice optical properties are quite different only in limited larger particle size ranges. The largest differences in the mass extinction coefficient (Figure 2d) are found for effective radii larger than 100 μm and for frequencies higher than 50 GHz. Differences in the single-scattering albedo (Figure 2e) are large at lower frequencies (<50 GHz) when effective radius is large (>200 μm), and a positive difference of about 0.4 remains around 30 μm for higher frequencies (>50 GHz).

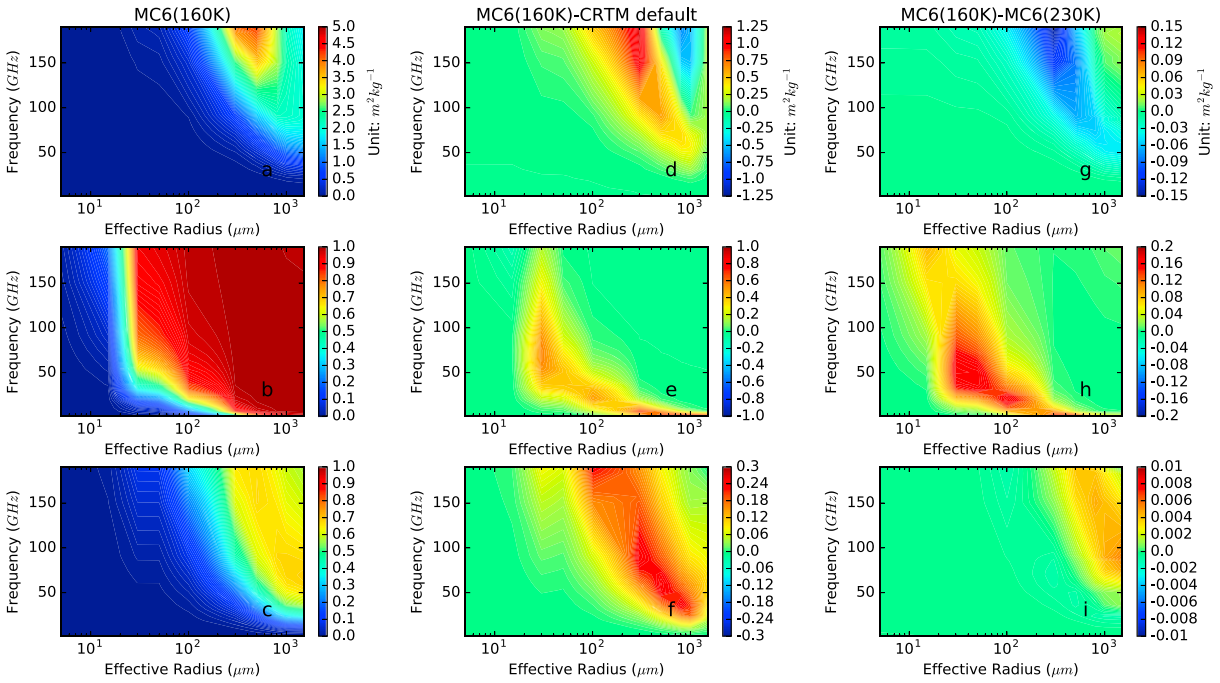

Figure 2. Comparison of bulk optical properties between the new MC6 ice cloud model and the CRTM default spherical ice cloud in the microwave region: (a) mass extinction coefficient, (b) single-scattering albedo, (c) asymmetry factor, (d–f) the corresponding MC6 minus CRTM differences of Figures 2a–2c, and (g–i) the corresponding MC6 at 160 K minus at 230 K differences of Figures 2a–2c.

The asymmetry factor difference (Figure 2f) is largest at effective radii varying from 1000 μm to 100 μm as the frequency increases.

Figures 2g–2i also show that the MC6 microwave ice optical properties are sensitive to temperature only in limited particle size ranges. In particular, with large particles at a cold temperature (160 K), the mass extinction coefficient is slightly smaller and the asymmetry factor is slightly larger than at 230 K. However, the single-scattering albedo is up to 0.2 larger at 160 K than at 230 K for moderate effective radii (30 μm to 60 μm). These results clearly show the complex dependencies of microwave ice cloud optical properties on temperature, size, and frequency.

Figure 3 shows all MC6 scattering phase matrix components for ice particles with effective radius of 800 μm at 10.7 GHz and 89 GHz frequencies. The scattering phase function (P_{11}), or the light scattering intensity at different scattering angles, typically has a large peak in the forward direction, indicating that forward scattering is much stronger than side and back scattering. However, the phase function at 10.7 GHz is almost constant at all scattering angles. This feature agrees with the fact that asymmetry factor at this size and frequency is close to 0 (see Figure 2c). For ice crystals at this size, the forward scattering peak at 89 GHz is about 1 order of magnitude larger than at 10.7 GHz. The other components of the scattering phase matrix are not used in this study but are provided for future development and applications of CRTM involving polarization. Temperature does not have a substantial impact on the scattering phase matrices at these two frequencies.

The ice cloud optical property LUT for the CRTM also contains Legendre expansions of the scattering phase function with 4, 6, 8, and 16 streams to meet different accuracies required when using the model. This is done by employing the δ-fit method [*Hu et al.*, 2000] to truncate the strong forward scattering peak and to reduce the number of terms needed to represent the phase function. After truncation, the optical thickness and the single-scattering albedo should be adjusted accordingly as described in *Yi et al.* [2014b].

3. Results and Discussions

3.1. Narrowband Simulation

Validation of a realistic case is made by comparison with observations from MODIS instrument on board the Aqua satellite. Specifically, a granule from the Aqua MODIS observation at 08:00 UTC 18 October 2013 over

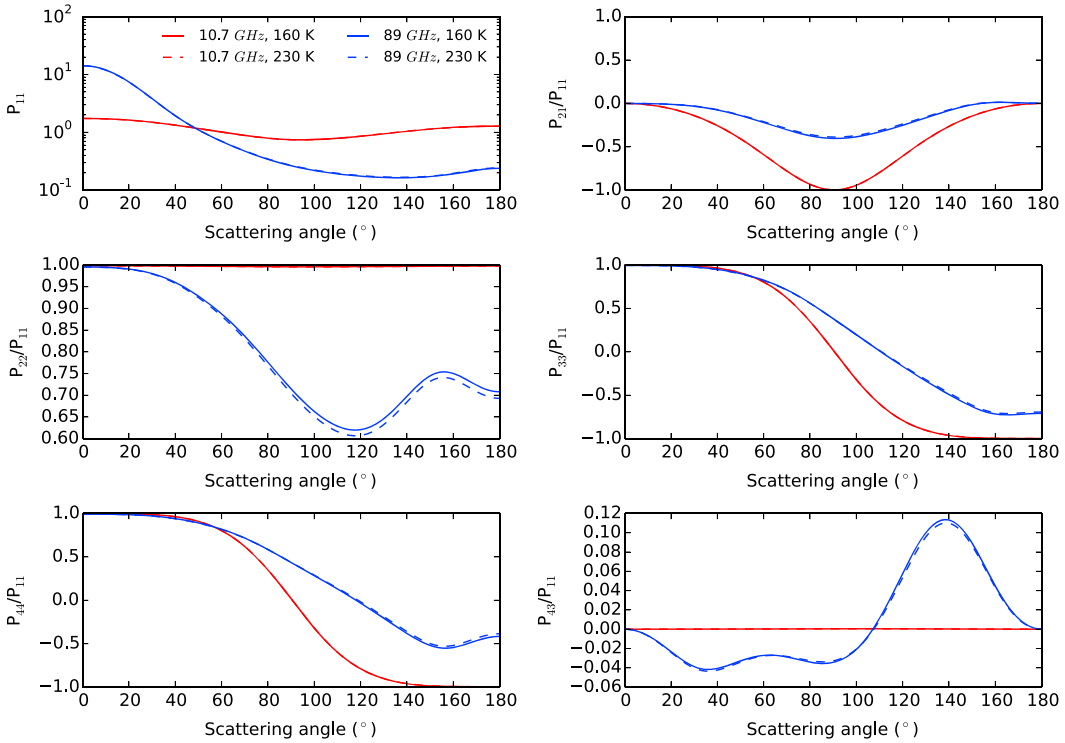

Figure 3. Scattering phase matrix of the MC6 ice cloud model for particles with an effective radius of 800 μm at frequencies of 10.7 and 89 GHz and at temperatures of 160 and 230 K.

the Indian Ocean that is predominantly covered by ice clouds is selected. We use the MODIS level 2 cloud phase product to select ice cloud pixels and then extract single-layer ice cloud pixels using the multilayer cloud flag. The single-layer ice cloud property retrievals (i.e., cloud top pressure, cloud effective radius, cloud optical depth, and ice water path) from MC6 are shown in Figure 4. Ice clouds are very complicated; in that, they have very different optical thicknesses with wide ranges of particle sizes at various height levels. The ice cloud top pressure ranges from 100 to 400 hPa, and the effective radius ranges from about 10 to 60 μm. For example, ice clouds near the edge of the cloud layer to the south of the equator (around 2°S, 80°E) have relatively lower cloud tops and smaller cloud particle effective radii. The cloud height, effective particle size, and optical thickness all have considerable impacts on the cloud radiance simulations. Due to the large number of ice cloud pixels within the MODIS granule, we only select a 10° × 10° domain from 5°S to 5°N and 75°E to 85°E (red box in Figure 4d) for detailed validation. This small region features some optically thick ice clouds at the center and in the northeast quadrant, some large particle effective radius ice clouds in the southwest quadrant, and a mixture of scattered high and low ice cloud tops. These well represent the intricacy of ice clouds, so a larger-scale intercomparison is not likely to show substantially different results.

Here we perform validation with the operational MODIS cloud retrievals from collection 6 or collection 5 as inputs and use the CRTM with either the MC6 or MC5 LUT to simulate brightness temperatures (BTs) in selected MODIS bands. Comparison with observations validates both the realism of the ice cloud model (assessed next) and the accuracy of the operational MODIS retrievals (assessed by a simple sensitivity analysis at the end of this section).

Figure 5 compares the observed and simulated brightness temperatures from MODIS channels 29 (8.55 μm) and 32 (12.02 μm) with the default MC5 and new MC6 ice optical property LUTs over the 10° × 10° domain region. It is evident that MC6 remarkably improves the ice cloud simulation capability of CRTM. The MC6 simulations capture the observed feature that bands at longer wavelengths (i.e., band 32) generally have lower BTs than those at shorter wavelengths (i.e., band 29; figures not shown). In the areas with thin ice clouds and low cloud tops, such as the southeast quadrant of the domain, the BTs can be as high as 280 K, while the thick ice clouds with high cloud tops can have BTs as low as 200 K. The MC5-simulated BTs are apparently lower than the observations overall. Although considerably improved, the MC6 BTs still have a

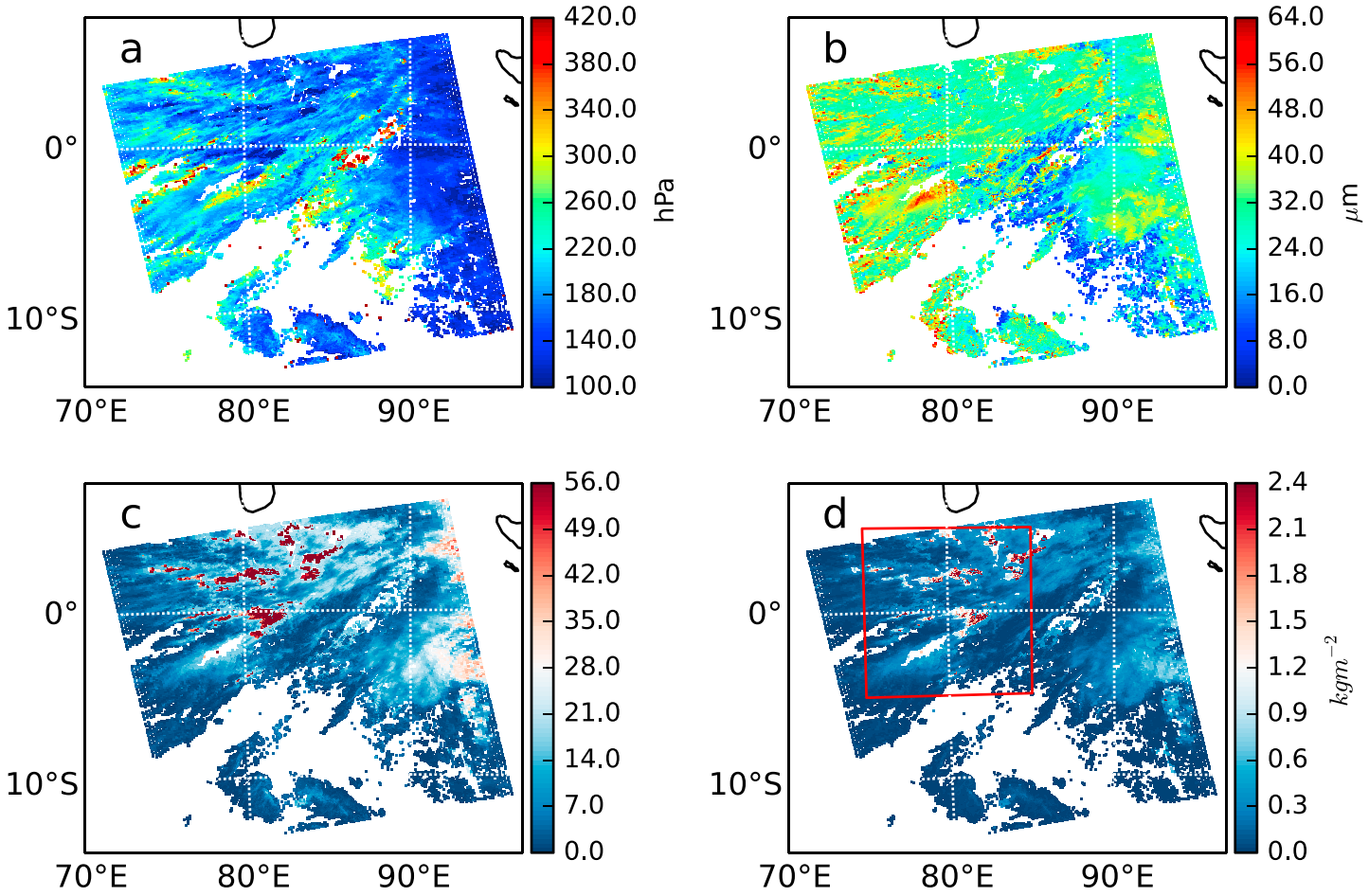

Figure 4. Ice cloud physical and optical properties in an Aqua MODIS granule (08:00 UTC 18 October 2013) from the operational MODIS collection 6 retrieval: (a) cloud top pressure, (b) ice particle effective radius, (c) cloud optical depth, and (d) ice water path.

slight cold bias (−4 K on average). This, however, can be due to many reasons other than the ice cloud property LUT.

A direct comparison of the performance of MC6 versus MC5 is shown in Figure 6. Scatterplot shows that the MC5-simulated BTs are mostly below the 1:1 line, indicating that BT simulations are largely underestimated in both MODIS bands 29 and 32. To be clearer, we define the brightness temperature difference (BTD) and the relative brightness temperature difference (RBTD) between CRTM and satellite observation as

$$\mathrm{BTD} = \mathrm{BT}_{\mathrm{CRTM}} - \mathrm{BT}_{\mathrm{OBS}}, \tag{3}$$

$$\mathrm{RBTD} = \mathrm{BTD}/\mathrm{BT}_{\mathrm{OBS}} \times 100\%, \tag{4}$$

where $\mathrm{BT}_{\mathrm{CRTM}}$ and $\mathrm{BT}_{\mathrm{OBS}}$ are the BTs from the CRTM simulation and satellite observation in the selected bands, respectively.

The domain mean BTD and RBTD in band 29 are −3.9 K and −1.64% with the MC6 LUT case and −17.3 K and −7.14% for the MC5 LUT case. The standard deviation decreases from 10.93 K and 4.04% in the MC5 case to 5.74 K and 2.36% in the MC6 case. In band 32, the above values are −2.18 K and −0.88% with MC6 and −13.0 K and −5.44% with MC5, and the standard deviation reduction is from 10.02 K and 3.84% with MC5 to 5.7 K and 2.36% with MC6. The other MODIS bands (results not shown) also show similar reductions in the BTD and RBTD. The improvements associated with the MC6 ice model in comparison with the MC5 counterpart can be partially attributed to the better physical and spectral consistencies that MC6 can provide when it is used for cloud property retrieval and radiative transfer simulation involving ice clouds.

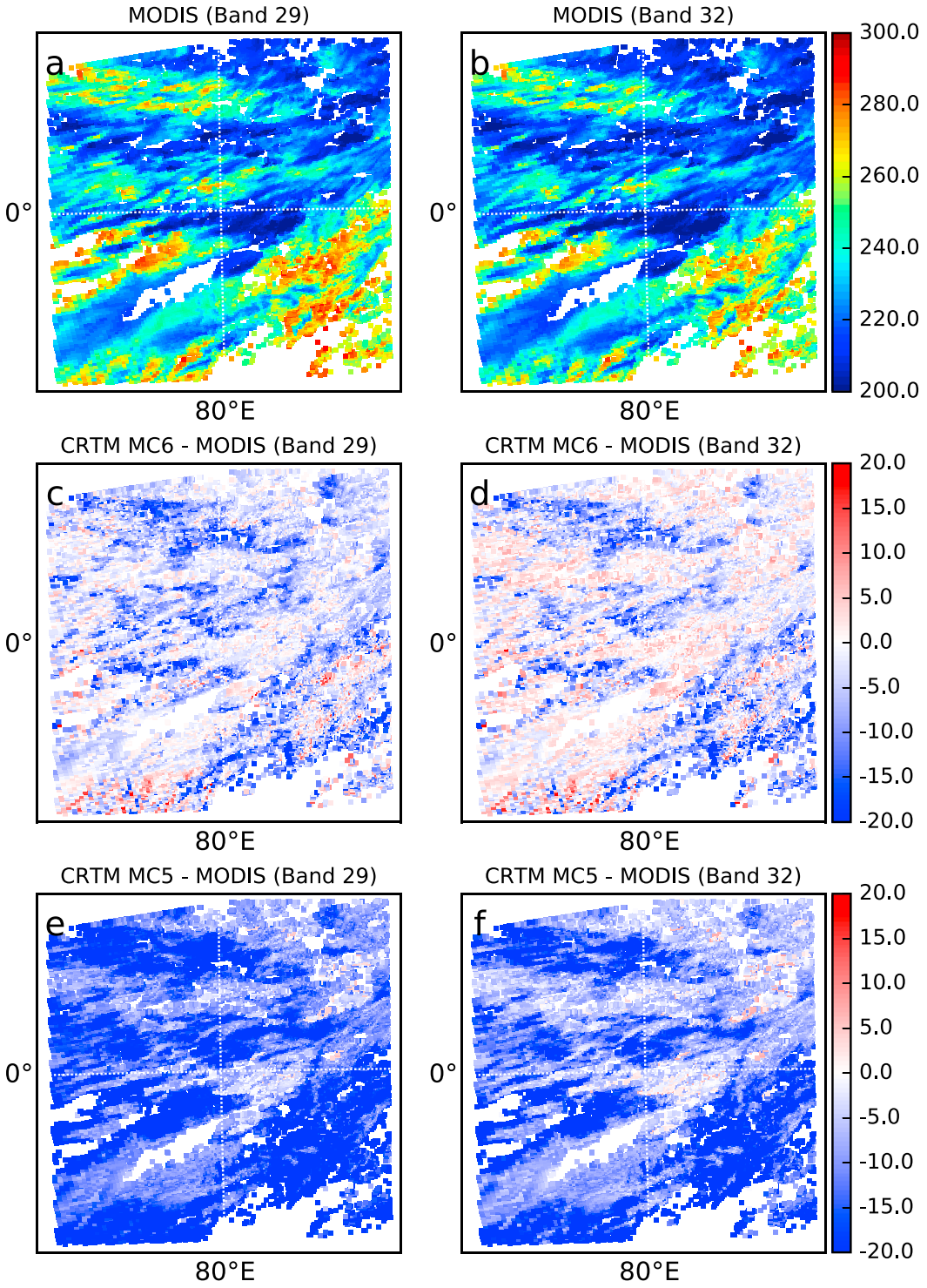

Figure 5. Comparison of observed and simulated brightness temperatures from two MODIS channels in bands (a, c, and e) 29 and (b, d, and f) 32. (Figures 5a and 5b) MODIS-observed BT, (Figures 5c and 5d) CRTM-simulated BT with MC6 LUT, and (Figures 5e and 5f) CRTM-simulated BT with default MC5 LUT.

While validation of MODIS retrievals of ice cloud properties (i.e., ice particle effective radius, ice water path, and cloud top pressure) is beyond the scope of this research, we perform a series of simple sensitivity analyses to investigate the possible impacts of errors in cloud properties. The input cloud properties are not exact because they are derived from satellite retrievals and may contain biases. Here they are perturbed by ±5%,

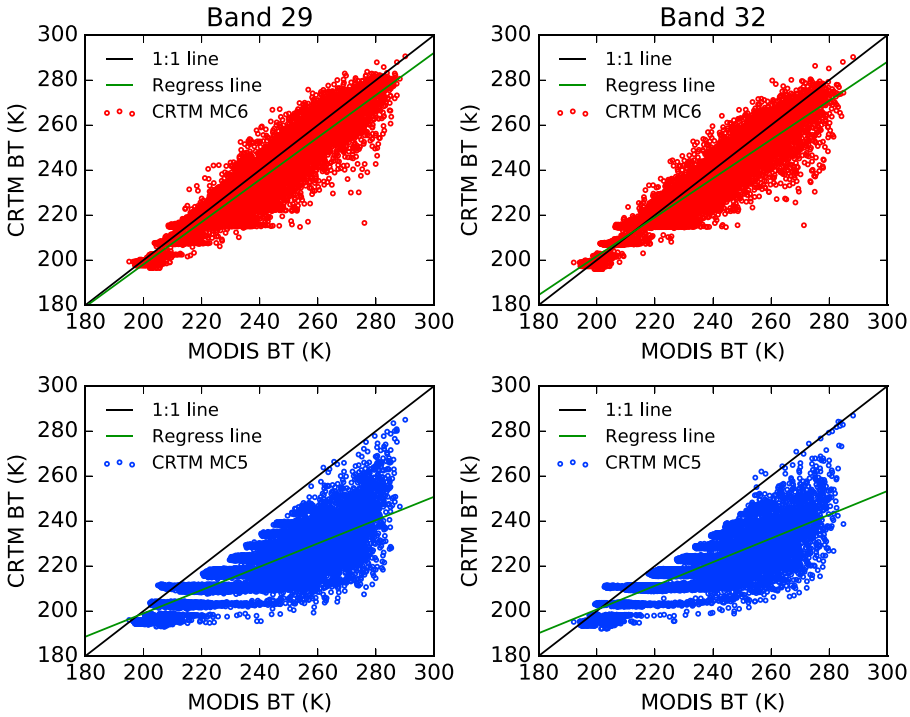

Figure 6. Scatterplot of observed and simulated brightness temperatures with default MC5 ice optical property LUT (blue) and the new MC6 LUT (red). (left) MODIS band 29 and (right) MODIS band 32.

and the mean BTD (perturbed minus unperturbed MC6 case) is calculated for each case. A 5% bias in the cloud retrieval products is a relatively acceptable quality threshold. Table 1 gives a summary of the results from the sensitivity tests with the mean and standard deviation of the BTDs shown.

A ±5% perturbation in ice particle effective radius or ice water path causes similar BTD magnitudes (~0.5 K) but with opposite signs. For example, an increased ice particle effective radius leads to a positive BTD while an increased ice water path results in a negative BTD. Their standard deviations are also around 0.5 K, which indicates that the BT uncertainty ranges are within 0~1 K.

Compared with the above cases, ±5% changes in cloud top pressure have larger impacts on the BTD, and a decrease of cloud top pressure (increased cloud top height) causes a larger negative BTD than an equal pressure increase. This is partially because the equal pressure changes represent unequal changes in altitude. However, both raised and lowered cloud layer cases have similar standard deviation of 2–3 K.

3.2. Hyperspectral Simulation in the IR Region

In *Yi et al.* [2014b], we compared simulated BTs in the Cross-track Infrared Sounder spectral channels between CRTM and the rigorous method. Here we compare the CRTM simulation with the AIRS hyperspectral observations using both MC6 and MC5 cloud products and LUTs.

Table 1. Summary of Brightness Temperature Changes in K (Relative to the Unperturbed Case) in MODIS Bands 29 and 32 for the 10° × 10° Domain in the Sensitivity Test Using MC6 LUT[a]

Perturbation		MODIS Band 29	MODIS Band 32
Ice particle effective radius	+5%	0.49 (0.52)	0.44 (0.52)
	−5%	−0.53 (0.56)	−0.46 (0.55)
Ice water path	+5%	−0.53 (0.50)	−0.41 (0.46)
	−5%	0.58 (0.52)	0.45 (0.49)
Cloud top pressure	+5%	0.81 (2.07)	0.90 (2.21)
	−5%	−2.78 (2.84)	−3.14 (3.01)

[a]The quantities in the parentheses are the corresponding standard deviation.

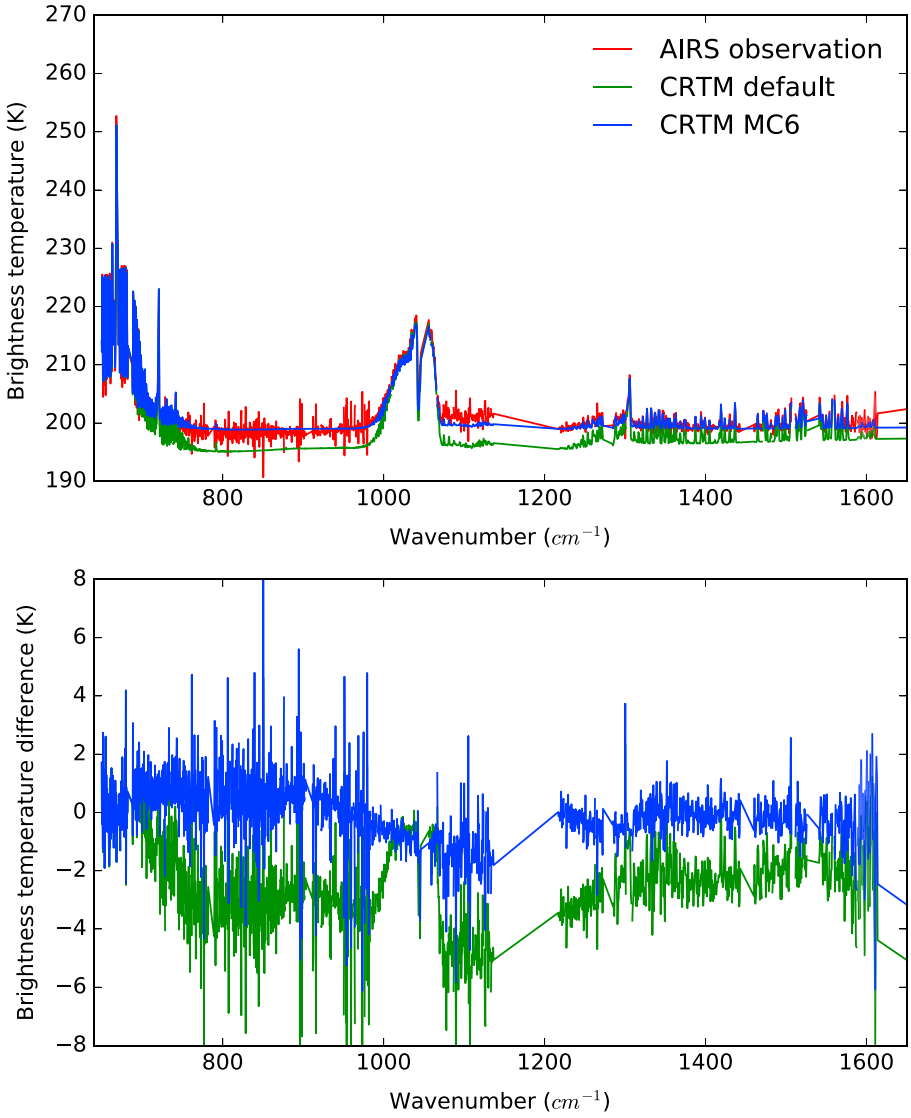

Figure 7. Comparison of observed and simulated brightness temperatures using CRTM with MC6 and default ice cloud optical properties at the longwave IR band of the AIRS instrument. The bottom plot shows the CRTM simulation minus the AIRS observation difference.

One point (0.0°S, 81.91°E) of a collocated cloudy sky observation of MODIS and AIRS located within the granule described above is chosen. The MC6 cloud top pressure, ice particle effective radius, and ice water path are 160.0 hPa, 30.66 μm, and 0.81 kg m^{-2}, respectively. The MC5 cloud top pressure, ice particle effective radius, and ice water path are 160.0 hPa, 24.34 μm, and 0.83 kg m^{-2}, respectively. The model settings are kept the same as the above simulation except that the viewing zenith and azimuthal angle are from the AIRS product.

Comparisons between simulated and observed brightness temperatures from 650 to 1650 cm^{-1} at a spectral interval of about 0.24 cm^{-1} are shown in Figure 7. Generally, the CRTM MC6 simulation result shows much better consistency with the AIRS observation than the MC5 simulation in the whole spectral range. BTDs for MC6 case are below 2 K except for the spikes, which are likely due to instrument noise or other factors, while BTDs for MC5 are mostly over twice as large. The differences in cloud retrieval properties between MC5 and MC6 are not substantial (except for the ice particle effective size), indicating the advantage of a physically and spectrally consistent ice model (i.e., MC6) particularly for hyperspectral radiance simulations.

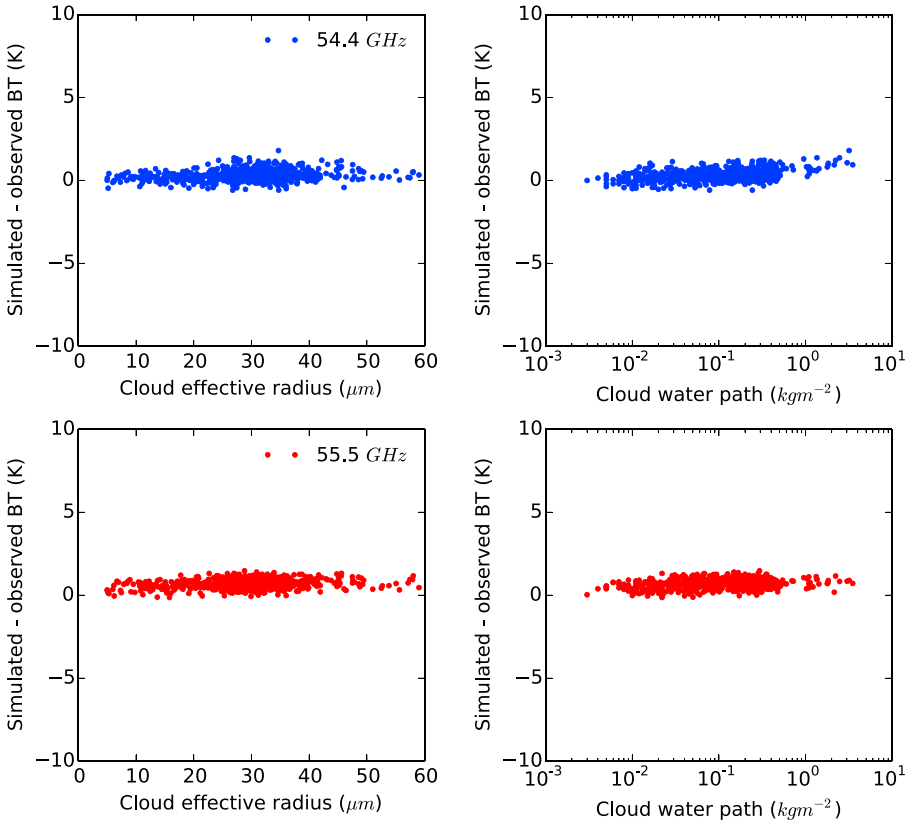

Figure 8. Brightness temperature difference between CRTM MC6 simulation and AMSU-A observation at (top) 54.4 GHz and (bottom) 55.5 GHz as functions of ice particle effective radius and ice water path.

3.3. Microwave Channel Simulations

It is also important to validate the performance of the new MC6 ice particle model in the microwave region. For this purpose, we collocate AMSU-A and MODIS observations on board the Aqua satellite in the same MODIS granule described above. Because MODIS has much finer resolution than AMSU-A, all ice cloudy MODIS pixels within a 20 km radius of the AMSU-A pixel are used in the CRTM simulation of brightness temperature. Finally, the averaged BT over those MODIS cloudy pixels is compared with the AMSU-A BT. Figure 8 shows the BTDs between the simulation and observation at 54.4 and 55.5 GHz as functions of ice particle effective radius and ice water path. The BTs at these two frequencies are well above 200 K. Thus, it is found that the CRTM MC6 simulations match quite well with the AMSU-A observations. It is also important to note that different ice particle models (such as MC5) and temperatures do not substantially affect the CRTM performance (figures not shown) at these two frequencies. This is partially due to the fact that these ice clouds have relatively small particle size (effective radius $<$60 μm), whereas differences in ice optical properties are more evident for relatively large particles (effective radius $>$100 μm).

4. Conclusions

In this study, we improved the ice cloud optical property look-up tables (LUTs) in the Community Radiative Transfer Model toward reducing the inaccuracy of the ice cloudy sky radiance simulation. The new ice particle model and ice particle size distribution are the same as the respective counterparts used in the present MODIS collection 6 ice cloud retrieval. Bulk spectral optical properties are calculated and parameterized as functions of cloud particle effective radius and are organized as look-up tables and implemented in CRTM. We have shown that the CRTM simulations with the new ice cloud LUTs are more accurate in a series of case studies.

A real Aqua MODIS granule with a wide range of single-layer ice cloud is selected to set up CRTM simulation. CRTM simulations are made using both CRTM default MC5 and the new MC6 ice cloud optical property LUTs in MODIS channels. BTs simulated by the CRTM with the new MC6-based LUT are much more realistic than BTs simulated using the default MC5 LUT, which show a persistent cold bias. Ice cloud properties (ice particle effective radius, ice water path, and cloud top pressure) used to simulate BTs for this validation are from operational retrievals, a process which is subject to errors. So an error sensitivity test assuming ±5% perturbations in each property is performed. It is found that errors in the ice particle effective radius and ice water path cause similar errors in simulated BTs, while cloud top pressure errors cause much larger BT errors, especially for underestimated cloud top pressures (or overestimated cloud top heights). The better representation of ice scattering properties provided by the MC6 ice cloud model allows for better cloud property retrievals and thus, better BT simulations when using consistent MC6 cloud products and MC6 LUT than the counterparts using those of MC5.

Hyperspectral simulation results calculated by using the CRTM are compared with AIRS observations in the range of 650 to 1650 cm^{-1}. The new MC6 ice cloud optical property LUTs nearly eliminate the cold bias of BTs simulated with the MC5 LUTs. Simulations of BTs in two microwave channels of the AMSU-A instrument also show excellent agreement with observations.

This study represents one step forward toward a better representation of ice cloud optical properties within the CRTM. We find that it is similarly important to have more accurate ice cloud property retrievals in order to simulate brightness temperature precisely. Although noticeable improvements in the simulation of brightness temperature are achieved in this study, it should be noted that large standard deviations of brightness temperature differences between simulation and observation still exist (see Figure 6). This implies that further investigations are needed to reduce the uncertainty of brightness temperature simulations. In particular, additional in situ observations are necessary to gain an improved understanding of ice habits and size distributions toward developing an optimal ice cloud model. More in-depth comparisons with other observational and modeling results should be conducted in the future.

Acknowledgments
This study is supported by NOAA grant NA15NES4400003. The Aqua MODIS level 2, collection 6 products were downloaded from the NASA Goddard Space Flight Center Level 1 and Atmosphere Archive and Distribution System (publicly available for download at https://ladsweb.nascom.nasa.gov/data/). Aqua AIRS and AMSU-A level 1B data can be downloaded through the Goddard Earth Sciences Data and Information Services Center (http://disc.sci.gsfc.nasa.gov/datacollection/AIRXBCAL_V005.html and http://disc.sci.gsfc.nasa.gov/datacollection/AIRABRAD_V005.html). The authors are grateful to Shouguo Ding and Yong Chen for their helpful discussions. A portion of the simulations was carried out at the Texas A&M University Supercomputing Facilities. The views expressed in this paper reflect the opinion of the authors and do not represent the U.S. government.

References

Baran, A. J., P. Hill, K. Furtado, P. Field, and J. Manners (2014), A coupled cloud physics-radiation parameterization of the bulk optical properties of cirrus and its impact on the Met Office Unified Model Global Atmosphere 5.0 configuration, *J. Clim.*, *27*, 7725–7752, doi:10.1175/JCLI-D-13-00700.1.

Baum, B. A., A. J. Heymsfield, P. Yang, and S. T. Bedka (2005), Bulk scattering properties for the remote sensing of ice clouds. Part 1: Microphysical data and models, *J. Appl. Meteorol. Climatol.*, *44*, 1885–1895, doi:10.1175/JAM2308.1.

Baum, B. A., P. Yang, A. J. Heymsfield, C. Schmitt, Y. Xie, A. Bansemer, Y. X. Hu, and Z. Zhang (2011), Improvements to shortwave bulk scattering and absorption models for the remote sensing of ice clouds, *J. Appl. Meteorol. Climatol.*, *50*, 1037–1056, doi:10.1175/2010JAMC2608.1.

Bi, L., and P. Yang (2014), Accurate simulation of the optical properties of atmospheric ice crystals with invariant imbedding T-matrix method, *J. Quant. Spectrosc. Radiat. Transfer*, *138*, 17–35, doi:10.1016/j.jqsrt.2014.01.013.

Bi, L., P. Yang, G. W. Kattawar, B. A. Baum, Y. X. Hu, D. M. Winker, R. S. Brock, and J. Q. Lu (2009), Simulation of the color ratio associated with the backscattering of radiation by ice particles at the wavelengths of 0.532 and 1.064 mm, *J. Geophys. Res.*, *114*, D00H08, doi:10.1029/2009JD011759.

Bi, L., P. Yang, G. W. Kattawar, and M. I. Mishchenko (2013), Efficient implementation of the invariant imbedding T-matrix method and the separation of variables method applied to large nonspherical inhomogeneous particles, *J. Quant. Spectrosc. Radiat. Transfer*, *116*, 169–183, doi:10.1016/j.jqsrt.2012.11.014.

Bi, L., P. Yang, C. Liu, B. Yi, B. A. Baum, B. van Diedenhoven, and H. Iwabuchi (2014), Assessment of the accuracy of the conventional ray-tracing technique: Implications in remote sensing and radiative transfer involving ice clouds, *J. Quant. Spectrosc. Radiat. Transfer*, *146*, 158–174, doi:10.1016/j.jqsrt.2014.03.017.

Ding, S., P. Yang, F. Weng, Q. Liu, Y. Han, P. van Delst, J. Li, and B. Baum (2011), Validation of the Community Radiative Transfer Model, *J. Quant. Spectrosc. Radiat. Transfer*, *112*, 1050–1064, doi:10.1016/j.jqsrt.2010.11.009.

Ebert, E. E., and J. A. Curry (1992), A parameterization of ice cloud optical properties for climate models, *J. Geophys. Res.*, *97*, 3831–3836, doi:10.1029/91JD02472.

Evans, K. F., and G. L. Stephens (1995), Microwave radiative transfer through clouds composed of realistically shaped ice crystals. Part I: Single scattering properties, *J. Atmos. Sci.*, *52*, 2041–2057, doi:10.1175/1520-0469(1995)052<2041:MRTTCC>2.0.CO;2.

Evans, K. F., S. J. Walter, A. J. Heymsfield, and M. N. Deeter (1998), Modeling of submillimeter passive remote sensing of cirrus clouds, *J. Appl. Meteorol.*, *37*, 184–205, doi:10.1175/1520-0450(1998)037<0184:MOSPRS>2.0.CO;2.

Foot, J. S. (1988), Some observations of the optical properties of clouds. Part II: Cirrus, *Q. J. R. Meteorol. Soc.*, *114*, 145–164, doi:10.1002/qj.49711447908.

Fu, Q. A. (1996), An accurate parameterization of the solar radiative properties of cirrus clouds for climate models, *J. Clim.*, *9*, 2058–2082, doi:10.1175/1520-0442(1996)009<2058:AAPOTS>2.0.CO;2.

Fu, Q., and K. N. Liou (1993), Parameterization of the radiative properties of cirrus clouds, *J. Atmos. Sci.*, *50*, 2008–2025, doi:10.1175/1520-0469(1993)050<2008:POTRPO>2.0.CO;2.

Han, Y., et al. (2006), Community Radiative Transfer Model (CRTM): Version 1 NOAA Techn. Rep., 122 pp., NOAA, Washington, D. C.

Heymsfield, A. J., C. Schmitt, and A. Bansemer (2013), Ice cloud particle size distributions and pressure-dependent terminal velocities from in situ observations at temperatures from 0° to −86°C, *J. Atmos. Sci.*, *70*, 4123–4154, doi:10.1175/JAS-D-12-0124.1.

Hong, G. (2007a), Parameterization of scattering and absorption properties of nonspherical ice crystals at microwave frequencies, *J. Geophys. Res.*, *112*, D11208, doi:10.1029/2006JD008364.

Hong, G. (2007b), Radar backscattering properties of nonspherical ice crystals at 94 GHz, *J. Geophys. Res.*, *112*, D22203, doi:10.1029/2007JD008839.

Hong, G., P. Yang, B. A. Baum, A. J. Heymsfield, F. Weng, Q. Liu, G. Heygster, and S. A. Buehler (2009), Scattering database in the millimeter and submillimeter wave range of 100–1000 GHz for nonspherical ice particles, *J. Geophys. Res.*, *114*, D06201, doi:10.1029/2008JD010451.

Hu, Y. X., B. Wielicki, B. Lin, G. Gibson, S.-C. Tsay, K. Stanmnes, and T. Wong (2000), δ-Fit: A fast and accurate treatment of particle scattering phase functions with weighted singular-value decomposition least-squares fitting, *J. Quant. Spectrosc. Radiat. Transfer*, *65*, 681–690, doi:10.1016/S0022-4073(99)00147-8.

Iwabuchi, H., and P. Yang (2011), Temperature dependence of ice optical constants: Implications for simulating the single-scattering properties of cold ice clouds, *J. Quant. Spectrosc. Radiat. Transfer*, *112*, 2520–2525, doi:10.1016/j.jqsrt.2011.06.017.

King, M. D., S. Platnick, G. Wind, G. T. Arnold, and R. T. Dominguez (2010), Remote sensing of the radiative and microphysical properties of clouds during TC4: Results from MAS, MASTER, MODIS, and MISR, *J. Geophys. Res.*, *115*, D00J07, doi:10.1029/2009JD013277.

Liou, K. N. (1986), Influence of cirrus clouds on weather and climate processes—A global perspective, *Mon. Weather Rev.*, *114*, 1167–1199, doi:10.1175/1520-0493(1986)114<1167:IOCCOW>2.0.CO;2.

Liu, C., P. Yang, P. Minnis, N. Loeb, S. Kato, A. Heymsfield, and C. Schmitt (2014), A two-habit model for the microphysical and optical properties of ice clouds, *Atmos. Chem. Phys.*, *14*, 13,719–13,737, doi:10.5194/acp-14-13719-2014.

Liu, G. (2008), A database of microwave single-scattering properties for nonspherical ice particles, *Bull. Am. Meteorol. Soc.*, *89*, 1563–1570, doi:10.1175/2008BAMS2486.1.

Liu, Q., and F. Weng (2006), Advanced doubling-adding method for radiative transfer in planetary atmosphere, *J. Atmos. Sci.*, *63*, 3459–3465, doi:10.1175/JAS3808.1.

Lynch, D. K., K. Sassen, D. O. Starr, and G. Stephens (2002), *Cirrus*, pp. 480 , Oxford Univ. Press, New York.

Macke, A., J. Mueller, and E. Raschke (1996), Single scattering properties of atmospheric ice crystals, *J. Atmos. Sci.*, *52*, 2813–2825, doi:10.1175/1520-0469(1996)053<2813:SSPOAI>2.0.CO;2.

McFarquhar, G. M., P. Yang, A. Macke, and A. J. Baran (2002), A new parameterization of single-scattering solar radiative properties for tropical ice clouds using observed ice crystal size and shape distributions, *J. Atmos. Sci.*, *59*, 2458–2478.

Menzel, W. P., R. A. Frey, H. Zhang, D. P. Wylie, C. C. Moeller, R. E. Holz, B. Maddux, B. A. Baum, K. I. Strabala, and L. E. Gumley (2008), MODIS global cloud-top pressure and amount estimation: Algorithm description and results, *J. Appl. Meteorol. Climatol.*, *47*(4), 1175–1198, doi:10.1175/2007JAMC1705.1.

Mishchenko, M. I., and L. D. Travis (1998), Capabilities and limitations of a current FORTRAN implementation of the T-matrix method for randomly oriented, rotationally symmetric scatterers, *J. Quant. Spectros. Radiat. Transfer*, *60*, 309–324, doi:10.1016/S0022-4073(98)00008-9.

Mitchell, D. L., A. Macke, and Y. G. Liu (1996), Modeling cirrus clouds. 2. Treatment of radiative properties, *J. Atmos. Sci.*, *53*, 2967–2988, doi:10.1175/1520-0469(1996)053<2967:MCCPIT>2.0.CO;2.

Nasiri, S. L., B. A. Baum, A. J. Heymsfield, P. Yang, M. R. Poellot, D. P. Kratz, and Y. Hu (2002), The development of midlatitude cirrus models for MODIS using FIRE-I, FIRE-II, and ARM in situ data, *J. Appl. Meteorol.*, *41*, 197–217.

Platnick, S., M. D. King, S. A. Ackerman, W. P. Menzel, B. A. Baum, J. C. Riedi, and R. A. Frey (2003), The MODIS cloud products: Algorithms and examples from Terra, *IEEE Trans. Geosci. Remote Sens.*, *41*(2), 459–473, doi:10.1109/TGRS.2002.808301.

Platnick, S., M. D. King, K. G. Meyer, G. Wind, N. Amarasinghe, B. Marchant, G. T. Arnold, Z. Zhang, P. A. Hubanks, B. Ridgway, and J. C. Riedi (2015), MODIS cloud optical properties: User guide for the collection 6 level-2 MOD06/MYD06 product and associated level-3 datasets, Version 1.0, 141 pp. [Available at http://modis-atmos.gsfc.nasa.gov/_docs/C6MOD06OPUserGuide.pdf.]

Rienecker, M. M., et al. (2011), MERRA: NASA's Modern-Era Retrospective Analysis for Research and Applications, *J. Clim.*, *24*, 3624–3648, doi:10.1175/JCLI-D-11-00015.1.

Schmitt, C. G., and A. J. Heymsfield (2007), On the occurrence of hollow bullet rosette- and column-shaped ice crystals in midlatitude cirrus, *J. Atmos. Sci.*, *64*, 4514–4519, doi:10.1175/2007JAS2317.1.

Schneider, T. L., and G. L. Stephens (1995), Theoretical aspects of modeling backscattering by cirrus ice particles at millimeter wavelengths, *J. Atmos. Sci.*, *52*, 4367–4385, doi:10.1175/1520-0469(1995)052<4367:TAOMBB>2.0.CO;2.

Takano, Y., and K. N. Liou (1989), Solar radiative transfer in cirrus clouds. Part I: Single-scattering and optical properties of hexagonal ice crystals, *J. Atmos. Sci.*, *46*, 3–19, doi:10.1175/1520-0469(1989)046<0003:SRTICC>2.0.CO;2.

Ulanowski, Z., E. Hesse, P. H. Kaye, and A. J. Baran (2006), Light scattering by complex ice-analogue crystals, *J. Quant. Spectrosc. Radiat. Transfer*, *100*, 382–392, doi:10.1016/j.jqsrt.2005.11.052.

Ulanowski, Z., E. Hirst, P. H. Kaye, and R. Greenaway (2012), Retrieving the size of particles with rough and complex surfaces from two-dimensional scattering patterns, *J. Quant. Spectrosc. Radiat. Transfer*, *113*, 2457–2464, doi:10.1016/j.jqsrt.2012.06.019.

Um, J., and G. M. McFarquhar (2007), Single-scattering properties of aggregates of bullet rosettes in cirrus cloud, *J. Appl. Meteorol. Climatol.*, *46*, 757–775, doi:10.1175/JAM2501.1.

Um, J., and G. M. McFarquhar (2009), Single-scattering properties of aggregates of plates, *Q. J. R. Meteorol. Soc.*, *135*, 291–304, doi:10.1002/qj.378.

van Diedenhoven, B., A. S. Ackerman, B. Cairns, and A. M. Fridlind (2014), A flexible parameterization for shortwave optical properties of ice crystals, *J. Atmos. Sci.*, *71*, 1763–1782, doi:10.1175/JAS-D-13-0205.1.

Warren, S. G. (1984), Optical constants of ice from the ultraviolet to the microwave, *Appl. Opt.*, *23*, 1206–1225.

Warren, S. G., and R. E. Brandt (2008), Optical constants of ice from the ultraviolet to the microwave: A revised compilation, *J. Geophys. Res.*, *113*, D14220, doi:10.1029/2007JD009744.

Yang, P., and K. N. Liou (1996a), Geometric-optics-integral-equation method for light scattering by nonspherical ice crystals, *Appl. Opt.*, *35*, 6568–6584, doi:10.1364/AO.35.006568.

Yang, P., and K. N. Liou (1996b), Finite-difference time domain method for light scattering by small ice crystals in three-dimensional space, *J. Opt. Soc. Am. A*, *13*, 2072–2085, doi:10.1364/JOSAA.13.002072.

Yang, P., and K. N. Liou (1998), Single-scattering properties of complex ice crystals in terrestrial atmosphere, *Contrib. Atmos. Phys.*, *71*, 223–248.

Yang, P., B. A. Baum, A. J. Heymsfield, Y. X. Hu, H.-L. Huang, S.-C. Tsay, and S. Ackerman (2003), Single-scattering properties of droxtals, *J. Quant. Spectrosc. Radiat. Transfer*, *79-80*, 1159–1180, doi:10.1016/S0022-4073(02)00347-3.

Yang, P., L. Bi, B. A. Baum, K. N. Liou, G. W. Kattawar, M. I. Mishchenko, and B. Cole (2013), Spectrally consistent scattering, absorption, and polarization properties of atmospheric ice crystals at wavelengths from 0.2 to 100 μm, *J. Atmos. Sci.*, *70*, 330–347, doi:10.1175/JAS-D-12-039.1.

Yang, P., K. N. Liou, L. Bi, C. Liu, B. Q. Yi, and B. A. Baum (2015), On the radiative properties of ice clouds: Light scattering, remote sensing, and radiation parameterization, *Adv. Atmos. Sci.*, *32*(1), 32–63, doi:10.1007/s00376-014-0011-z.

Yee, S. K. (1966), Numerical solution of initial boundary value problems involving Maxwell's equations in isotropic media, *IEEE Trans. Antennas Propag.*, *14*, 302–307.

Yi, B., P. Yang, B. A. Baum, T. L'Ecuyer, L. Oreopoulos, E. J. Mlawer, A. J. Heymsfield, and K.-N. Liou (2013), Influence of ice particle surface roughening on the global cloud radiative effect, *J. Atmos. Sci.*, *70*, 2794–2807, doi:10.1175/JAS-D-13-020.1.

Yi, B., X. Huang, P. Yang, B. A. Baum, and G. W. Kattawar (2014a), Considering polarization in MODIS-based cloud property retrievals by using a vector radiative transfer code, *J. Quant. Spectrosc. Radiat. Transfer*, *146*, 540–548, doi:10.1016/j.jcprt.2014.05.020.

Yi, B., P. Yang, F. Weng, and Q. Liu (2014b), Assessment and validation of the community radiative transfer model for ice cloud conditions, Proc. SPIE 9259, Remote Sensing of the Atmosphere, Clouds, and Precipitation V, 92591C, doi:10.1117/12.2069341.

Yurkin, M. A., V. P. Maltsev, and A. G. Hoekstra (2007), The discrete dipole approximation for simulation of light scattering by particles much larger than the wavelength, *J. Quant. Spectrosc. Radiat. Transfer*, *106*, 546–557, doi:10.1016/j.jqsrt.2007.01.033.

Zhang, Z., P. Yang, G. W. Kattawar, S.-C. Tsay, B. A. Baum, H.-L. Huang, Y. X. Hu, A. J. Heymsfield, and J. Reichardt (2004), Geometric optics solution to light scattering by droxtal ice crystals, *Appl. Opt.*, *43*, 2490–2499, doi:10.1364/AO.43.002490.